RSC Advances

PAPER

View Article Online
View Journal | View Issue

Cite this: *RSC Adv.*, 2019, **9**, 27476

Dual recognition of Al^{3+} and Zn^{2+} ions by a novel probe based on diarylethene and its application†

Yaping Zhang, Hui Li, * Wendan Gao and Shouzhi Pu*

Received 22nd July 2019
Accepted 20th August 2019

DOI: 10.1039/c9ra05652a

rsc.li/rsc-advances

We synthesized a new fluorescent probe **1O** by attaching a diarylethene molecule to a functional group. The probe can be used to detect Al^{3+} and Zn^{2+} at the same time with high selectivity, and its detection limit is very low. When Al^{3+} was added, the fluorescence intensity was increased 310 folds, and was accompanied by a fluorescent color change from black to grass-green. Similarly, after the addition of Zn^{2+}, the fluorescence intensity was enhanced 110 folds, with a concomitant color change from black to yellow-green. Moreover, based on the properties of **1O**, we designed a logic circuit, and that also can be used for water sample testing.

Introduction

Small anions, metal cations, and neutral molecules participate in different biological activities and play various important roles in human metabolism.[1] Among many metals, aluminum is the most abundant metallic element in the Earth's crust,[2,3] and its compounds are widely used in dye production, and the paper and food industries.[4–6] Aluminum is not a necessary element for the functioning of the human body, and it may accumulate in the organs and tissues for a long time before it is excreted, so the excessive and deficiency of aluminum will result negative effects on the human body.[7–10] For instance, aluminum is linked to Alzheimer's disease, Parkinson's disease, amyotrophic lateral sclerosis, colic, rickets, gastrointestinal problems, interference with the metabolism of calcium, and memory loss.[11–15] Thus, aluminum is toxic to biological systems, but it is widely found in the biosphere. It is therefore generally valuable to synthesize a probe that can detect Al^{3+} with high accuracy.

Zinc is one of the transition metals in the human body found in quantities second only to iron, and due to its biological significance, a large body of research exists for zinc.[6–18] It is well known that zinc exists in various enzymes and has multiple functions in basic biological processes, such as apoptosis, gene transcription, immune function, pathology, muscle contraction, neural signal transmission, and immune function.[19–21] Therefore, the correct amount of zinc in the body is also important.[22,23] As reported, a healthy human body should contain 200 to 300 mg of zinc, and a deficiency in zinc can cause physical growth retardation and nervous system disorders.[24–26] Zinc can also cause some diseases, such as cerebral ischemia and Alzheimer's disease, amyotrophic lateral sclerosis, Parkinson's disease, and hypoxia-ischemia.[27–30] An excess of zinc can contribute to superficial skin diseases, diabetes, and brain disease.[31–33] Thus, it is imperative to use efficient tools to detect zinc to confirm the existence of proper levels.

There are numerous methods used to detect Al^{3+} and Zn^{2+}, such as chromatography, potentiometric ion-selective electrodes, *et al.*[34–36] However, they have some disadvantages compared to a fluorescent probe.[37–39] Fluorescent probes have the merits of low cost, fast response, real-time detection, and high selectivity and sensitivity.[40,41] Therefore, in recent years, there has been wide usage of fluorescent probes because they have been proven to be one of the most useful detection tools. Additionally, due to their cost-effectiveness and real-time application, there is greater interest in synthesizing single fluorescent probes for simultaneous multi-target detection.[42,43] For reported probes based on diarylethene, most of them can only recognize one ion, and their detection limit is not low enough.[44–47] There are probes that can simultaneously detect Al^{3+} and Zn^{2+}, and even in two solvents,[48] but they are rare. There are many other probes that can simultaneously detect Al^{3+} and Zn^{2+},[49–54] and although they can simultaneously detect ions in a mixture of solvents, the detection limit is not low enough. Here, we synthesized a probe that could be used to simultaneously detect Al^{3+} and Zn^{2+}, and because it has a low detection limit, it has great application prospects for multi-ion detection.

In recent years, great progress has been made in the study of molecular logic gates, and it is important to design molecules for molecular logic devices that can respond to specific ion inputs.[55] Therefore, many fundamental logic gates such as a key-pad lock, multiplexer, encoder/decoder, and molecular-scale computer have been designed *via* fundamental molecules.[56,57] As a result, molecular logic gates that respond to chemicals and biological input signals have attracted great

Jiangxi Key Laboratory of Organic Chemistry, Jiangxi Science and Technology Normal University, Nanchang 330013, P. R. China. E-mail: lihui5626@163.com; pushouzhi@tsinghua.org.cn; Fax: +86-791-83831996; Tel: +86-791-83831996

† Electronic supplementary information (ESI) available. See DOI: 10.1039/c9ra05652a

interest.[58] Among many photochromic materials, diarylethene has proven to be very useful because of its unique structure and excellent photochromic properties.[59–61] Based on diarylethene, a series of probes for detecting various ions was synthesized by linking diarylethene to functional groups, such as pyrazole. Pyrazole compounds widely exist in nature and exhibit many unique biological activities and coordination functions, some of which can be used in clinical treatment.[62–64] In materials science, pyrazole compounds are widely used in transition metal and rare earth organic fluorescent materials due to their coordination function.[65,66]

Based on the above, we were designed and synthesized a novel fluorescent probe based on a diarylethene derivative and a pyrazole functional group. The probe can detect and distinguish Al^{3+} and Zn^{2+} from each other with high selectivity and sensitivity. The properties of the probe and its selectivity towards Al^{3+} and Zn^{2+} were systematically investigated, and it was determined that it can detect Al^{3+} and Zn^{2+} by fluorescence enhancement. Also, its structure was characterized by ^{1}H and ^{13}C nuclear magnetic resonance (NMR) spectroscopy, and electrospray ionization-mass spectrometry (ESI-MS). A diagram of its photochromism is shown in Scheme 1.

Experimental

General methods

The chemicals used in these experiments were purchased from J&K Chemicals and Innochem Technology, and used directly without further purification. All of the solvents were analytical grade and purified by distillation before use. The ionic solutions used in the experiments were prepared by dissolving metal salts of various ions in deionized water. Among them, only Ba^{2+}, K^{+}, Sn^{2+}, and Hg^{2+} ions are metal chlorides; the others are metal nitrates. The EDTA disodium salt solution was also dissolved in deionized water. NMR spectra were obtained with a Bruker AV400 (400 MHz) spectrometer using DMSO-d_6 as the solvent and tetramethylsilane as the internal standard. UV/Vis absorption spectra were measured on an Agilent 8453 UV/Vis spectrophotometer. Fluorescent spectra were recorded with a Hitachi F4600 fluorescence spectrophotometer. The mass spectra were measured using a Bruker Amazon SL Ion Trap mass spectrometer. Elemental analysis was carried out with a PE CHN 2400 analyzer, and the melting point was measured with a WRS-1B melting point apparatus. The lighting devices used in the experiment were a MUL-165 UV lamp and a MVL-210 visible lamp.

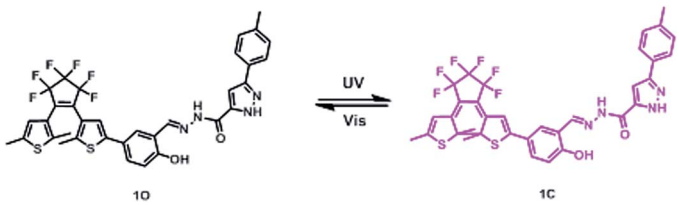

Scheme 1 Photochromism of diarylethene **1O**.

Sample pretreatment

The water samples analysed included tap water and water from Yaohu Lake in Nanchang, China. Water samples were filtered through a 0.2 mm membrane filter to remove suspended particulate matter before analysis. Then, Al^{3+} and Zn^{2+} were added to form a solution of a certain concentration.

Synthesis of the target compound

The route for synthesizing the target compound, 1-(2,5-dimethyl-3-thienyl)-2-{2-methyl-5-[4-hydroxyl-3-(3-(4-methylphenyl)-1*H*-pyrazole-5-carbohydrazide)phenyl]-3-thienyl}perflurocyclopentene is shown in Scheme 2 (**1O**). Compounds **2** and **3** were facilely synthesized in high yield according to previously published procedures.[67]

Weighed compound **3** was added to a 25 ml single-mouth bottle, and a syringe was used to add 5 ml of absolute ethanol. Then, compound **4** was added to the solution, which was heated and refluxed for 7 h. The mixture was cooled to room temperature, and then stored in a refrigerator overnight. Purification was performed by recrystallization of the anhydrous ethanol, and target compound **1O** was obtained as a white solid with a yield of 79%; mp 523–524 K. Anal. calcd. for $C_{32}H_{22}F_6N_2O_3S_2$ (%): calcd: C, 58.28; H, 3.74; N, 8.0; O, 4.57; found: C, 58.60; H, 3.42; N, 8.09; O, 4.48. ^{1}H NMR (DMSO-d_6, 400 MHz), δ (ppm): 1.87 (s, 3H), 1.91 (s, 3H), 2.35 (s, 3H), 2.42 (s, 3H), 6.85 (s, 1H), 7.00 (d, 1H), 7.19 (s, 1H), 7.31 (t, 2H), 7.38 (s, 1H), 7.57 (d, 1H), 7.75 (d, 3H), 8.76 (s, 1H), 11.59 (s, 1H), 12.20 (s, 1H), 13.80 (s, 1H). ^{13}C NMR (DMSO-d_6, 100 MHz), δ (ppm): 14.38, 15.15, 21.30, 103.64, 117.78, 119.94, 121.84, 124.03, 124.67, 124.86, 125.60, 125.88, 126.28, 126.42, 128.79, 130.08, 138.63, 140.08, 140.40, 141.77, 144.36, 146.68, 147.85, 157.90, 158.63. MS (ESI^{-}): m/z 699.1 $[M - H]^{-}$.

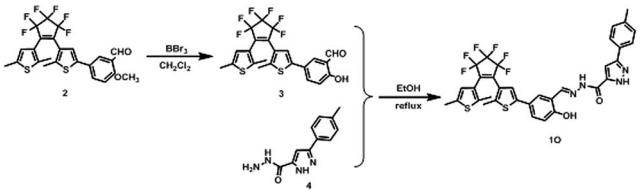

Scheme 2 Synthetic route of diarylethene **1O**.

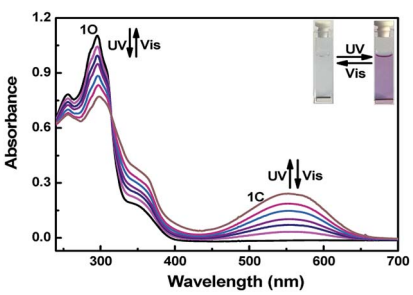

Fig. 1 Changes in the absorption spectra of **1O** upon alternating irradiation with UV and visible light in methanol (2.0×10^{-5} mol L^{-1}).

Results and discussion

Photochromic properties of 1O

The photochromic properties of **1O** were tested in methanol (2.0×10^{-5} mol L^{-1}) at room temperature and under UV light ($\lambda = 254$ nm) and visible light ($\lambda > 500$ nm). As shown in Fig. 1, a strong absorption peak was observed at 296 nm in the initial state, and the absorption peak would decrease with irradiation of 297 nm light, which may have been caused by the result of the $\pi \rightarrow \pi^*$ transition. Because of the appearance of closed-loop states **1C** with π-electron intramolecular delocalization,[68] a new absorption band appeared at 553 nm. At the same time, the color of the solution changed from colorless to purple. In contrast, using visible light ($\lambda > 500$ nm) to irradiate the solution of **1C**, the absorption peak returned to the initial state, and the color of the solution was entirely bleached. In general, the photochromic process of **1O** is a reversible process. When the photostationary state (PSS) was reached, a distinct isosbestic point of isomerization was observed at 322 nm, indicating that the photoisomerization was a unimolecular process of two species and supported the reversible two-component photochromic reaction scheme.[69]

Fluorescence response to metal ions

At room temperature, the selectivity of compound **1O** was measured in methanol. As Fig. 2A and B show, during excitation at 420 nm, when the same amount of various metal ions (Cu^{2+}, K^+, Ni^{2+}, Co^{2+}, Cd^{2+}, Ba^{2+}, Sn^{2+}, Mg^{2+}, Zn^{2+}, Hg^{2+}, Ca^{2+}, Mn^{2+}, Pb^{2+}, Sr^{2+}, Cr^{3+}, Al^{3+}, and Fe^{3+}) was added to solution **1O**, only the addition of Al^{3+} and Zn^{2+} resulted in dramatic enhancement of fluorescence intensity. When Al^{3+} was added, a strong emission peak appeared at 530 nm, and the intensity of the fluorescence was enhanced 310-fold compared to **1O**. The obvious change of color from black to grass-green may have

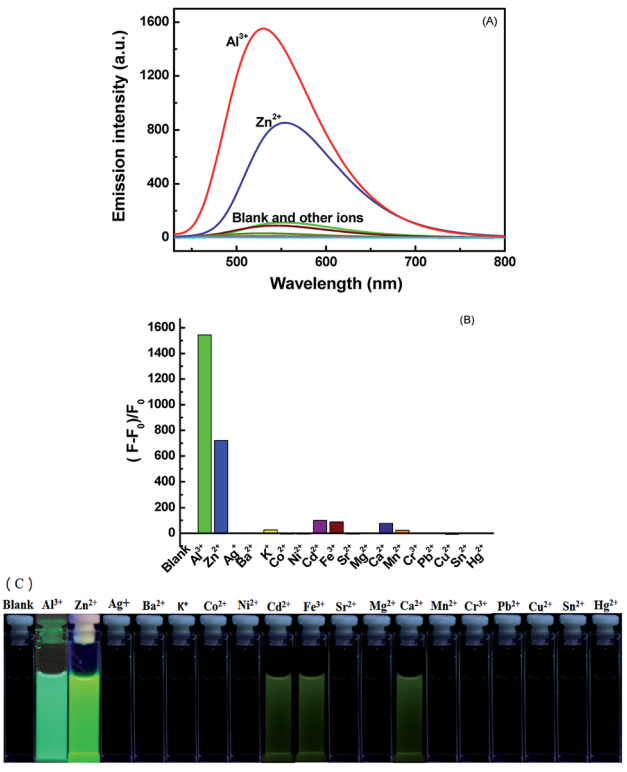

Fig. 2 Changes in the fluorescence of **1O** induced by the addition of various metal ions (5.0 equiv.) in (2.0×10^{-5} mol L^{-1}) methanol: (A) emission spectral changes, (B) emission intensity changes, and (C) photographs of fluorescence changes.

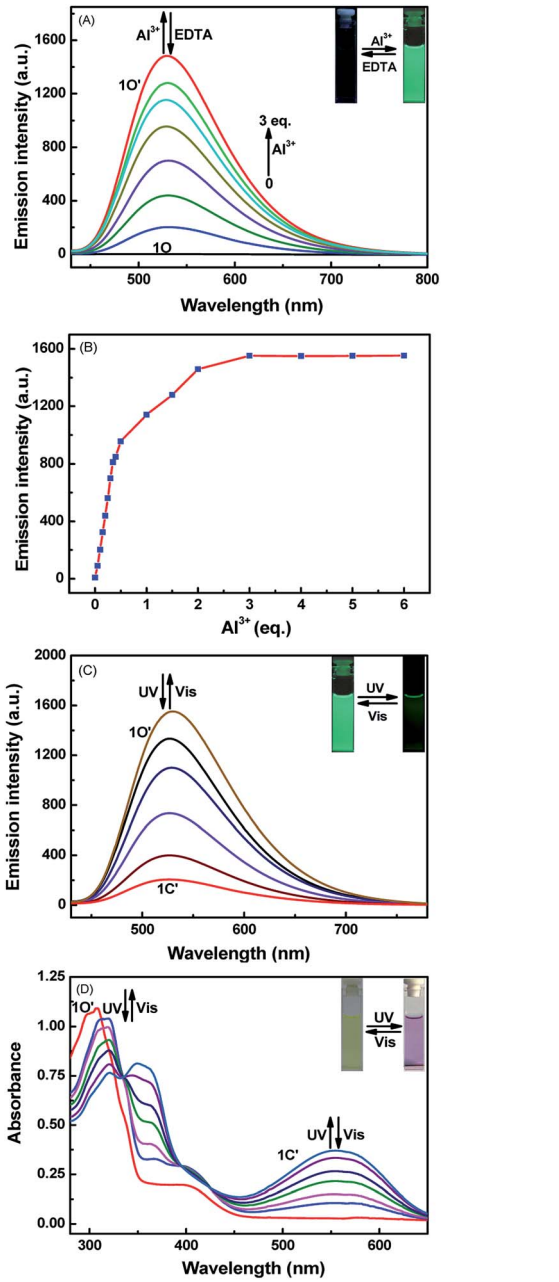

Fig. 3 Changes in the fluorescence of **1O** in methanol (2.0×10^{-5} mol L^{-1}) induced by Al^{3+}/EDTA and light stimuli at room temperature, excited at 420 nm: (A) emission intensity and fluorescence color changes of **1O** induced by the addition of Al^{3+}; (B) the curve of the fluorescent intensity ratio at 530 nm with the addition of different equiv. of Al^{3+} concentrations; (C) emission intensity and fluorescence color changes of **1O**–Al^{3+} by photoirradiation; and (D) changes in the absorption spectra and color of **1O** and **1O′** induced by UV/Vis light stimuli in methanol (2.0×10^{-5} mol L^{-1}).

been caused by the formation of **1O**–Al^{3+} (**1O′**). After Zn^{2+} was added, a strong emission peak appeared at 553 nm, and compared with **1O**, the intensity of the fluorescence increased by 110-fold. The change in the color from black to yellow green may be due to the **1O**–Zn^{2+} (**1O″**), as shown in Fig. 2C. Therefore, compound **1O** could be used to detect Al^{3+} and Zn^{2+} in the solution of methanol.

Fluorescence titration experiments were conducted in methanol at room temperature to determine the fluorescence response of Al^{3+}, Zn^{2+}, and UV/Vis. As Fig. 3A shows, with increasing Al^{3+} (0–3 eq.), the formation of **1O**–Al^{3+} increased and led to an increase in the fluorescence intensity, but when the amount of added Al^{3+} reached 3.0 eq., the fluorescence intensity tended to equilibrium and reached a maximum. In the entire process, the emission peak of **1O** blueshifted from 524 nm to 530 nm, and the fluorescence intensity increased by 310 fold. After the fluorescence intensity reached the maximum, an experiment was conducted to measure its reversibility. When a certain amount of EDTA was added, the state of **1O′** returned to that of the original, which suggests that EDTA can separate Al^{3+} from the complex, and it is a reversible process.

The addition of Zn^{2+} resulted in changes similar to those seen with Al^{3+}. As Fig. 4A shows, when the amount of zinc ions added was from 0 to 5 eq., the fluorescence gradually increased and finally reached equilibrium. This was attributed to the production of complex **1O**–Zn^{2+} (**1O″**), which caused the isomerization of C=N to be suppressed. In this process, the fluorescence intensity enhanced 110 fold, the solution of **1O** changed from black to yellow-green, and the emission peak redshifted from 524 nm to 554 nm. Then, when the aqueous solution of EDTA was added, the result is that EDTA separated Zn^{2+} from the complex (**1O″**), and the fluorescence spectrum was recovered to the state of **1O**, thus demonstrating that the process is reversible.

Fig. 3B and 4B was described the linear relationship between different Al^{3+} and Zn^{2+} concentrations and emission intensity at 530 nm and 553 nm. For Al^{3+}, the linearity range is 0–0.45 eq., and for Zn^{2+}, the linearity range is 0–0.35 eq. This shows that with increasing Al^{3+} and Zn^{2+}, the fluorescence intensity was enhanced until the maximum was reached. The sparse fluorescence of **1O** can be attributed to the isomerization of C=N, and after the addition of Al^{3+} and Zn^{2+}, the fluorescence intensity gradually increased. This increase in fluorescence intensity can be explained by chelation enhancing fluorescence (CHEF).

It is worth noting that due to the inhibition of C=N isomerization, the chelates **1O**–Al^{3+} and **1O**–Zn^{2+} exhibited obvious fluorescence switching performance under UV/Vis irradiation. As Fig. 3C shows, with irradiation at 297 nm, the fluorescence intensity gradually decreased until it reached a minimum, which may be the formation of **1C′**. The **1O′** intensity was quenched by approximately 87%, and the color of the solution also turned a dark green. However, under visible light irradiation (λ > 500 nm), the fluorescence intensity and solution color were recovered to the initial state. Similarly, as Fig. 4C shows, the fluorescence intensity of **1O″** decreased after irradiation of 297 nm. Compared with **1C″**, the **1O″** intensity was quenched by approximately 91%. However, after being exposed to visible

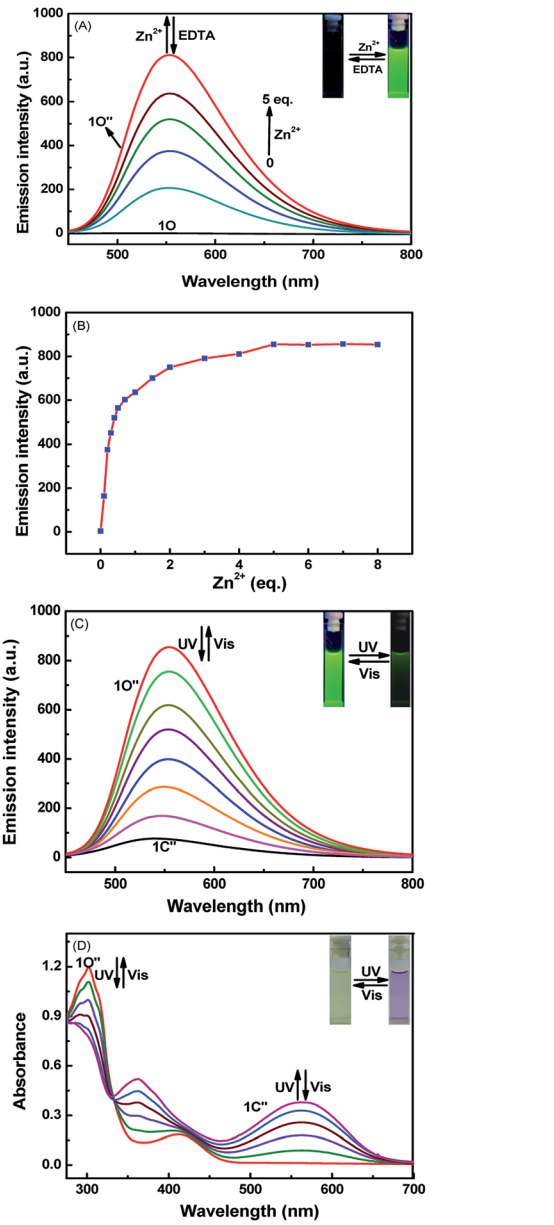

Fig. 4 Changes in the fluorescence of **1O** in methanol (2.0×10^{-5} mol L^{-1}) induced by Zn^{2+}/EDTA and light stimuli at room temperature, excited at 420 nm: (A) emission intensity and fluorescence color changes of **1O** induced by the addition of Zn^{2+}; (B) the curve of the fluorescent intensity ratio at 554 nm with the addition of different equiv. Zn^{2+} concentrations; (C) emission intensity and fluorescence color changes of **1O**–Zn^{2+} by photoirradiation; and (D) changes in the absorption spectra and color of **1O** and **1O″** induced by UV/Vis light stimuli in methanol (2.0×10^{-5} mol L^{-1}).

light (λ > 500 nm), the fluorescence intensity and solution color also returned to their initial state. Thus, from the above results, we can conclude that Al^{3+}, Zn^{2+}, EDTA, and UV/Vis light can be used to effectively modulate the fluorescence.

Additionally, a photochromic process experiment with **1O′** and **1O″** was conducted. As Fig. 3D shows, when **1O′** was irradiated with 297 nm light, the yellow solution would change to purple, and at 555 nm, a new peak was present and gradually increased until it reached a maximum. This occurred because of

a closed-loop reaction, and a closed-loop state of **1C′** was generated. The isosbestic point of the absorption spectrum appeared at 334 nm. For zinc, the result was the same (Fig. 4D). Under irradiation of 297 nm, the yellow color of the solution turns purple, and a new absorption peak was present at 563 nm; the isosbestic point was observed at 334 nm. However, when irradiated with visible light (λ > 500 nm), the spectrum and solution color of **1C′** and **1C″** all recovered to the initial state. Therefore, the photochromic process of **1O′** and **1O″** is reversible under UV and visible light.

In order to further determine the binding ability of **1O** to Al^{3+} and Zn^{2+}, Job's plot experiment was performed, and the results are shown in Fig. S3.† Under the premise of maintaining the total molar concentration of **1O** and Al^{3+} and Zn^{2+}, when the value of the emission intensity reached the maximum, the corresponding molar fraction is 0.5, and this illustrates that **1O** with Al^{3+} and Zn^{2+} are complexed in a 1 : 1 stoichiometry. As Fig. S4† shows, based on the fluorescence titration experiment of **1O** with Al^{3+} and Zn^{2+}, and according to the Benesi–Hildebrand equation, the complexation constant (K_a) of **1O** for Al^{3+} and Zn^{2+} was calculated, and it is 2.7×10^4 L mol^{-1} and 1.98×10^5 L mol^{-1}, respectively. The detection limit of compound **1O** for Al^{3+} and Zn^{2+} is 6.7×10^{-9} mol L^{-1} and 3.7×10^{-8} mol L^{-1}, respectively. This indicates that **1O** can be used to monitor Al^{3+} and Zn^{2+} with high accuracy.

It is well known that there are many fluorescent probes that have been reported to recognize Al^{3+} and Zn^{2+}, as shown in Table 1, which compares the detection limit of some probes. The table shows that the detection limit of this probe is not low enough. Here, the probe we designed can recognize both ions at the same time and has a low detection limit. Thus, the probe still has the advantage of recognizing Al^{3+} and Zn^{2+} at the same time.

Table 1 Comparison of other previous probes for the detection of Al^{3+} and Zn^{2+}

Sensor	LOD Al^{3+} (mol L^{-1})	LOD Zn^{2+} (mol L^{-1})	Ref.
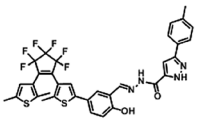	6.7×10^{-9}	3.7×10^{-8}	This work
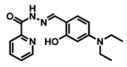	8.3×10^{-8}	1.24×10^{-7}	*J. Mater. Chem. B*, 2018
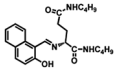	1.27×10^{-7}	5.5×10^{-8}	*Analytica Chimica Acta*, 2016
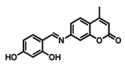	3.7×10^{-6}	3.86×10^{-6}	*Anal. Methods*, 2015
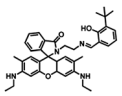	1.98×10^{-8}	7.69×10^{-8}	*ACS Omega*, 2019
	5.22×10^{-8}	7.88×10^{-8}	*Sens. Actuators, B*, 2018
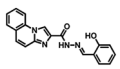	1.73×10^{-7}	6.36×10^{-8}	*RSC Adv.*, 2015
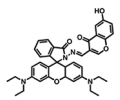	3.19×10^{-6}	1.25×10^{-7}	*Spectrochimica Acta A*, 2018
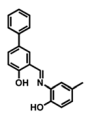	2.24×10^{-7}	0.41×10^{-7}	*New J. Chem.*, 2018
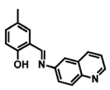	2.34×10^{-8}	5.37×10^{-8}	*Dalton Trans.*, 2018
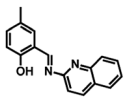	3.79×10^{-6}	13.6×10^{-8}	*Dalton Trans.*, 2018

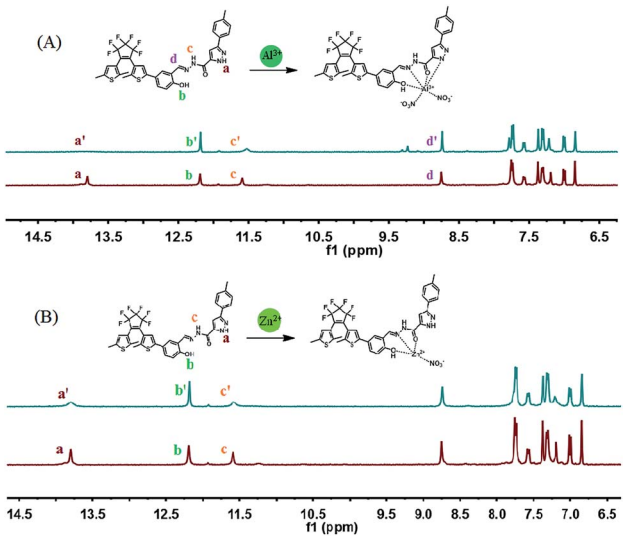

Fig. 5 (A) ^{1}H NMR spectra (400 MHz) measured during the titration of **1O** with Al^{3+} in DMSO-d_6. (B) ^{1}H NMR spectra (400 MHz) measured during the titration of **1O** with Zn^{2+} in DMSO-d_6.

In addition, the dates of mass spectrometry of **1O** with Al^{3+} and Zn^{2+} also proved the result of Job's plot experiment. As Fig. S5† shows, in the methanol solution of **1O**, a peak appeared at 699.1 m/z, which corresponds to $[\mathbf{1O}\text{–}H^+]^-$. When Al^{3+} was added, a new characteristic peak appeared at 762.0 m/z, which was due to the formation of $[\mathbf{1O} + Al^{3+} + 2NO_3^- - 2H^+]^-$. When Zn^{2+} was added to the solution of **1O**, a characteristic peak appeared at 762.9 m/z, which was assigned to $[\mathbf{1O} + Zn^{2+} + NO_3^- - 2H^+]^-$. Additionally, to further explore the combination method for **1O** with Al^{3+} and Zn^{2+}, ^{1}H NMR titration experiments were also conducted in DMSO-d_6 solvent. As Fig. 5A shows, with the addition of Al^{3+}, the H_a completely disappeared, which indicates that there is an interaction of Al^{3+}–N. The peak of H_b increased, which indicates that Al^{3+}–O was formed. The

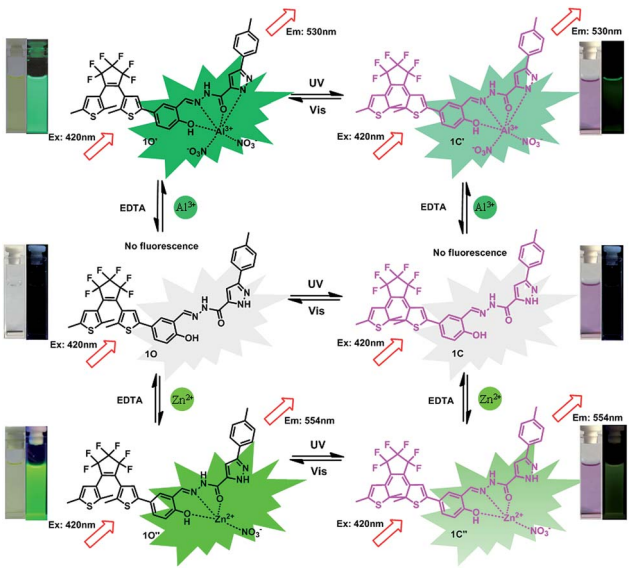

Scheme 3 Photochromism, color, and fluorescence changes of **1O** induced by Al^{3+}/EDTA, Zn^{2+}/EDTA, and UV/Vis lights.

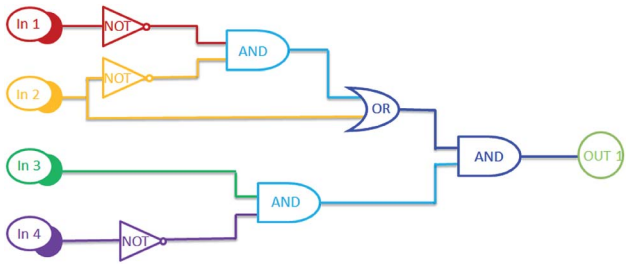

Fig. 6 The logic circuit based on the diarylethene molecule with various inputs: the combinational logic circuits equivalent to the truth table given in Table 2: In 1 (UV), In 2 (Vis), In 3 (Al^{3+}/Zn^{2+}), In 4 (EDTA), and OUT 1.

signal H_d was also enhanced, which indicates the form of Al^{3+}–N=. The H_c signal decreased, and shifted from 11.593 to 11.522, which may be affected by the interaction of Al^{3+}–O=. For Zn^{2+}, as Fig. 5B shows, upon the addition of Zn^{2+}, the peaks of Ha and H_c were significantly decreased. For the H_a, this denoted the generation of Zn^{2+}–O=, which will affect the change of H_a. For H_c, it also may be affected by the interaction of Zn–N=. However, the H_b was enhanced, which indicates that the interaction of Al–O occurred. Thus, the proposed sensing mechanism of Al^{3+} and Zn^{2+} by **1O** is shown in Fig. 5.

Application in logic circuits

On the basis of the experimental results, Al^{3+}, Zn^{2+}, and UV/Vis can effectively regulate the photochromic and fluorescence properties of **1O**. The photoswitching behaviour of compound **1O** is displayed in Scheme 3. Based on these properties of **1O**, a logic gate was designed. As shown in Fig. 6, the logic gate consists of four input values: UV (In 1), Vis (In 2), Al^{3+}/Zn^{2+} (In 3), and EDTA (In 4), and one output: the fluorescence intensity

Table 2 Truth table for all possible strings for four binary-input data points and the corresponding output digit of the photochromic behavior of **1O**[a]

Input				Output (λ_{em} = 530/554 nm)
In 1 (UV)	In 2 (Vis)	In 3 (Al^{3+}/Zn^{2+})	In 4 (EDTA)	
0	0	0	0	0
1	0	0	0	0
0	1	0	0	0
0	0	1	0	1
0	0	0	1	0
1	1	0	0	0
1	0	1	0	0
1	0	0	1	0
0	1	1	0	1
0	1	0	1	0
0	0	1	1	0
1	1	1	0	1
1	1	0	1	0
1	0	1	1	0
0	1	1	1	0
1	1	1	1	0

[a] When the emission intensity at 530/554 nm is more than 110 fold that of the original state, the output signal is defined as '1'; otherwise, it is defined as '0'.

Table 3 Detection of Al^{3+} in water samples[a]

Sample	Al^{3+} added (μM)	Al^{3+} determined (μM), *n*	Recovery (%)	RSD (%)
Yaohu lake	1	1.03	103	1.9
	2	2.08	105	1.45
	3	3.06	102	2
Tap water	1	0.96	96	4.1
	2	1.93	97	1.6
	3	2.93	98	1.1

[a] *n* = the average of the three tests.

Table 4 Detection of Zn^{2+} in water samples[a]

Sample	Zn^{2+} added (μM)	Zn^{2+} determined (μM), *n*	Recovery (%)	RSD (%)
Yaohu lake	1	1.05	105	1.9
	2	2.06	103	2.1
	3	3.05	102	1.5
Tap water	1	0.99	99	3
	2	1.94	97	2.1
	3	2.93	98	0.6

[a] *n* = the average of the three tests.

at 530/553 nm. For the input signal, when UV, Vis, Al^{3+}/Zn^{2+}, and EDTA exist, this is described as the "on" state. Conversely, the case where they do not exist is defined as the "off" state. That is, when the compound is irradiated with UV, it represents that the input signal In 1 is "on" or is "off". Vis (In 2), Al^{3+}/Zn^{2+} (In 3), and EDTA (In 4) are also the same. For the output signal, the fluorescence emission intensity of compound **1O** is considered to be "off" with the Boolean value "0". After addition of Al^{3+}/Zn^{2+}, the fluorescence intensity is increased by 310/110 times, which is considered to be "on", and the Boolean value is "1". All four possible inputs are shown in Table 2, and the corresponding logic circuit diagram is shown in Fig. 6.

Detecting Al^{3+} and Zn^{2+} in water

Considering the influence of Al^{3+}/Zn^{2+} on the human body and the environment, the capability of **1O** to detect Al^{3+}/Zn^{2+} in crude water samples was tested with standard methods to validate its practical utility in environmental science. Water samples were prepared as described in the experimental section. As depicted in Tables 3 and 4, after adding different concentrations of Al^{3+}/Zn^{2+} into the water sample, obvious fluorescence enhancement was observed, and the Al^{3+}/Zn^{2+} concentration in these water samples could be accurately measured by probe **1O**.[70,71] The result was the average of the three parallel experiments, and the relative standard deviation (RSD) was also calculated. As shown in Tables 3 and 4, the recovery rate of Al^{3+} was between 96% and 105%, and the recovery rate of Al^{3+} was between 97% and 105%.[72,73] Therefore, from the calculation results, **1O** can be used for the detection of actual water samples.

Conclusions

We have synthesized a fluorescent probe **1O** by attaching a diarylethene molecule to a functional group, and it can be used to detect Al^{3+} and Zn^{2+} at the same time by enhanced fluorescence intensity. When Al^{3+} was added, the fluorescence intensity increased 310 folds and was accompanied by a fluorescent color change from black to grass-green. Similarly, after the addition of Zn^{2+}, the fluorescence intensity was enhanced 110 folds, with a concomitant color change from black to yellow-green. The probe can simultaneously recognize Al^{3+} and Zn^{2+} and has a low detection limit. Moreover, based on the properties of **1O**, we have designed a logic circuit, and it also can be used for water sample testing. These results indicate that diarylethene-based fluorescent probes have great potential as a dual sensor.

Conflicts of interest

There are no conflicts of interest to declare.

Acknowledgements

The authors are grateful for financial support from the National Natural Science Foundation of China (21861017, 41867052, 41867053), the "5511" Science and Technology Innovation Talent Project of Jiangxi, and the Open Project Program of "311 High Level Engineering Center", Jiangxi Science & Technology Normal University (No. KFGJ19004).

Notes and references

1 L. Yu, S. L. Wang, K. Z. Huang, Z. G. Liu, F. Gao and W. B. Zeng, *Tetrahedron*, 2015, **71**, 4679.
2 L. K. Kumawat, M. Kumar and P. Bhatt, *Anal. Methods*, 2016, **8**, 7369.
3 M. Mukherjee, S. Pal and S. Lohar, *Analyst*, 2014, **139**, 4828.
4 A. S. M. Islama, R. Bhowmicka and H. Mohammada, *New J. Chem.*, 2016, **40**, 4710.
5 A. Gupta and N. Kumar, *RSC Adv.*, 2016, **6**, 106413.
6 S. Samanta, U. Manna and T. Ray, *Dalton Trans.*, 2015, **44**, 18902.
7 N. Behera and V. Manivannan, *J. Photochem. Photobiol., A*, 2018, **353**, 77.
8 E. Serkan and K. Ozcan, *Sens. Actuators, B*, 2018, **273**, 56.
9 Z. Shuang, J. L. Shi and J. S. Xue, *Spectrochim. Acta, Part A*, 2018, **205**, 276.
10 H. Y. Lei, H. P. Diao, W. Liu, J. Xie, Z. J. Wang and L. H. Feng, *RSC Adv.*, 2016, **6**, 77291.
11 J. Sun, Z. Liu and Y. Wang, *RSC Adv.*, 2015, **5**, 100873.
12 H. Li, J. Z. Wang and S. J. Zhang, *RSC Adv.*, 2018, **8**, 31889.
13 C. Kim, T. G. Jo and J. Lee, *New J. Chem.*, 2016, **40**, 8918.
14 G. Yang, X. Meng and Z. Z. Wang, *New J. Chem.*, 2018, **42**, 14630.
15 Y. Chen, Y. Mi and Q. Xie, *Anal. Methods*, 2013, **5**, 4818.
16 J. H. Kim, I. H. Hwang and S. P. Jang, *Dalton Trans.*, 2013, **42**, 5500.

17 S. BasuRoy, C. Prodhan and K. Chaudhuri, *Photochem. Photobiol. Sci.*, 2017, **14**, 1103.
18 L. Zhang, X. Cui and J. Sun, *Bioorg. Med. Chem. Lett.*, 2013, **23**, 3511.
19 M. Patil, S. Bothra, S. K. Sahoo, H. A. Rather, R. Vasita, R. Bendre and A. Kuwar, *Sens. Actuators, B*, 2018, **270**, 200.
20 X. X. He, X. M. Wang, L. Zhang, G. Z. Fang, J. F. Liu and S. Wang, *Sens. Actuators, B*, 2018, **287**, 289.
21 S. Sun, Q. Shu and P. Lin, *RSC Adv.*, 2016, **6**, 93826.
22 J. Li, Y. Chen and T. Chen, *Sens. Actuators, B*, 2018, **268**, 446.
23 H. Liu, Y. Tan and Q. Dai, *Dyes Pigm.*, 2018, **158**, 312.
24 Y. Kun, J. X. Fu and Y. X. Chang, *Spectrochim. Acta, Part A*, 2018, **205**, 410.
25 H. J. Jang, J. H. Kang and M. Lee, *Ind. Eng. Chem. Res.*, 2018, **57**, 54.
26 K. Aich, S. Goswami, S. Das and C. D. Mukhopadhyay, *RSC Adv.*, 2015, **5**, 31189.
27 S. Marzieh, A. Mehdi and M. Soraia, *New J. Chem.*, 2018, **42**, 12595.
28 J. M. Jung, J. H. Kang, J. Han, H. Lee, M. H. Lim, K. T. Kim and C. Kim, *Sens. Actuators, B*, 2018, **267**, 58.
29 J. H. Kang, J. Han and H. Lee, *Dyes Pigm.*, 2018, **152**, 131.
30 K. Du, S. Z. Niu and L. Qiao, *RSC Adv.*, 2017, **7**, 40615.
31 Z. L. Lu, Y. N. Lu and W. L. Fan, *Spectrochim. Acta, Part A*, 2019, **206**, 295.
32 F. G. Huo, Q. Wu, J. Kang, Y. B. Zhang and C. X. Yin, *Sens. Actuators, B*, 2018, **262**, 263.
33 L. Somenath, P. Siddhartha and M. Manjira, *RSC Adv.*, 2017, **7**, 25528.
34 P. Hou, J. Wang and S. Fu, *Anal. Bioanal. Chem.*, 2019, **411**, 935.
35 J. H. Hu, J. B. Li, J. Qi and J. J. Chen, *New J. Chem.*, 2015, **39**, 843–848.
36 Y. P. Xuan and J. B. Qu, *RSC Adv.*, 2018, **8**, 4125.
37 N. Thirumalaivasan, P. Venkatesan and S. P. Wu, *New J. Chem.*, 2017, **41**, 13510.
38 J. Li, C. Yin and T. Liu, *Sens. Actuators, B*, 2017, **252**, 1112.
39 J. Kang, F. J. Huo, Y. B. Zhang, J. B. Chao, T. E. Glass and C. X. Yin, *Spectrochim. Acta, Part A*, 2019, **209**, 95.
40 X. Ding, F. Zhang and Y. Bai, *Tetrahedron Lett.*, 2017, **58**, 3868.
41 H. Seo, M. An and B. Y. Kim, *Tetrahedron*, 2017, **73**, 4684.
42 B. Gu, L. Huang and W. Su, *Anal. Chim. Acta*, 2017, **954**, 97.
43 Y. Tang, Y. Y. Li, J. Han, Y. L. Mao, L. Ni and Y. Wang, *Spectrochim. Acta, Part A*, 2019, **208**, 299.
44 Z. L. Shi, Y. Y. Tu and S. Z. Pu, *RSC Adv.*, 2018, **8**, 6727.
45 E. T. Feng, C. B. Fan, N. S. Wang, G. Liu and S. Z. Pu, *Dyes Pigm.*, 2018, **15**, 22.
46 S. Q. Cui, S. Y. Qiu, R. M. Lu and S. Z. Pu, *Tetrahedron Lett.*, 2018, **59**, 3365.
47 R. J. Wang, L. Diao, Q. W. Ren, G. Liu and S. Z. Pu, *ACS Omega*, 2019, **4**, 309.
48 Z. Wang, S. Q. Cui, S. Y. Qiu and S. Z. Pu, *J. Photochem. Photobiol., A*, 2019, **376**, 185.
49 H. Y. Liu, T. Q. Liu, J. Li, *et al.*, *J. Mater. Chem. B*, 2018, **6**, 5435.
50 Y. Tang, J. Sun and B. Yin, *Anal. Chim. Acta*, 2016, **942**, 104.
51 H. Ananta, R. Ankita, M. Abhishek, *et al.*, *Dalton Trans.*, 2018, **47**, 13972.
52 J. C. Qi, L. Fan, B. D. Wang, *et al.*, *Anal. Methods*, 2015, **7**, 716.
53 A. Roy, U. Shee, A. Mukherjee, *et al.*, *ACS Omega*, 2019, **4**, 6864.
54 B. J. Pang, C. R. Li and Z. Y. Yang, *Spectrochim. Acta, Part A*, 2018, **59**, 929.
55 S. Karmakar, S. Mardanya, D. Maity, S. Baitalik, *et al.*, *Sens. Actuators, B*, 2016, **226**, 388.
56 Y. Han, Y. Niu, M. Liu, *et al.*, *J. Mater. Chem. B*, 2019, **7**, 897.
57 S. Erbas-Cakmak, S. Kolemen, A. C. Sedgwick, *et al.*, *Chem. Soc. Rev.*, 2018, **47**, 2228.
58 D. Mondal, P. Pal and S. Baitalik, *Sens. Actuators, B*, 2017, **242**, 746.
59 W. D. Gao, Y. P. Zhang, H. Li and S. Z. Pu, *Tetrahedron*, 2019, **75**, 2538.
60 L. H. Zhai, Y. Y. Tu, Z. L. Shi and S. Z. Pu, *Spectrochim. Acta, Part A*, 2019, **218**, 171.
61 F. F. Liu, C. B. Fan and S. Z. Pu, *J. Photochem. Photobiol., A*, 2019, **371**, 248.
62 J. M. Wolfand, G. H. LeFevre and R. G. Luthy, *Environ. Sci.: Processes Impacts*, 2016, **18**, 1256.
63 Y. Guo, X. G. Wang, L. L. Qu, S. N. Xu, Y. Zhao, R. Q. Xie, M. X. Huang and Y. B. Zhang, *RSC Adv.*, 2017, **7**, 11796.
64 H. G. Bonacorso, G. M. D. Forno, C. Wiethan, A. Ketzer, N. Zanatta, C. P. Frizzo, M. A. P. Martins and M. Stradiotto, *RSC Adv.*, 2017, **7**, 43957.
65 D. R. Boyd, N. D. Sharma, G. P. Coen, F. Hempenstall, V. Ljubez, J. F. Malone, C. C. R. Allen and J. T. G. Hamilton , *Org. Biomol. Chem.*, 2008, **6**, 3957.
66 V. Novohradsky, A. Zamora, A. Gandioso, V. Brabec, J. Ruiz and V. Marchán, *Chem. Commun.*, 2017, **53**, 5523.
67 W. D. Gao, Y. P. Zhang, H. Li and S. Z. Pu, *Tetrahedron*, 2018, **74**, 6299.
68 Q. H. You, P. S. Chan and W. H. Chan, *RSC Adv.*, 2012, **2**, 11078–11083.
69 S. Goswami, K. Aich, A. K. Das, A. Manna and S. Das, *RSC Adv.*, 2013, **3**, 2412.
70 L. Xiong, J. Ma, Y. Huang, *et al.*, *ACS Sens.*, 2017, **2**, 599.
71 Q. Sun, S. H. Yang, L. Wu, *et al.*, *Anal. Chem.*, 2016, **88**, 2266.
72 F. Tan, L. Cong, N. M. Saucedo, *et al.*, *J. Hazard. Mater.*, 2016, **320**, 226.
73 Z. Wang, D. M. Han, W. P. Jia, *et al.*, *Anal. Chem.*, 2012, **84**, 4915.